

## Supporting Documents

# UV-Initiated Self-Healing of Oxolane-Chitosan-Polyurethane (OXO-CHI-PUR) Networks

Biswajit Ghosh, Kishore V. Chellappan and Marek W. Urban\*

School of Polymers and High Performance Materials  
Shelby F. Thames Polymer Science Research Center  
The University of Southern Mississippi  
Hattiesburg, MS 39406

\*- to whom all correspondence should be addressed (E-mail: [marek.urban@usm.edu](mailto:marek.urban@usm.edu))

### **Synthesis of OXO-CHI Macromonomer**

Figure S1 illustrates a two-step reaction sequence leading to the OXO-CHI-PUR network synthesis. In the first step, CHI was dispersed in 50 % w/w NaOH solution at -5 °C for 24 h followed by -18 °C for 48 h. The reaction mixture was thawed to room temperature and reacted with tetrahydro-furfuryl chloride (OXO-Cl) to substitute the primary -OH groups of CHI in C<sub>6</sub> position with OXO ring as well as conversion of acetamide (-NHCOCH<sub>3</sub>) functionalities to -NH<sub>2</sub> groups. OXO-CHI was isolated from the reaction mixture by precipitation and washed with methanol to neutralize it. In the next step, OXO-CHI was dispersed in DMSO and reacted with trifunctional HDI monomer and polyethylene glycol (PEG) in presence of DBTDL catalyst, resulting formation of OXO-CHI-PUR networks.

In order to determine the attachment of 5-membered OXO ring at the backbone of CHI macromonomer ATR FT-IR and <sup>13</sup>C NMR analysis were conducted. As shown in Figure S2, Traces A and B represent FT-IR spectra of CHI and OXO-CHI respectively. As seen, the intensity of 1665 cm<sup>-1</sup> corresponding to -C=O stretching vibrations of acetamide groups of CHI decreases, at the same time the intensity of 1580 cm<sup>-1</sup> corresponding to amide I increases in

Trace B compared to Trace A. These observations suggest the conversion of acetamide groups into amide groups under experimental condition. On the other hand, new bands appear at 1326, and 1080  $\text{cm}^{-1}$  corresponding to  $-\text{CH}_2-$  deformation vibration and  $-\text{C}-\text{O}-\text{C}-$  stretching vibration of OXO suggesting OXO ring attachment at the backbone of CHI.

Again, to confirm the incorporation of OXO ring within CHI backbone Figure S3, Traces A and B represent  $^{13}\text{C}$  NMR spectra of CHI and OXO-CHI, respectively. In Trace A characteristics resonances due to carbonyl carbon (a) of acetamide group in glycosine units and carbon (b) attributed to the methyl of  $-\text{NHCOCH}_3$  group at 175 and 22.5 ppm are detected, respectively. These resonances are not detected in Trace B due to the conversion of acetamide into primary amine groups and give rise to new resonances at 33 and 24 ppm which correspond to carbon atoms (a) and (b) of OXO ring, respectively.

### **Micro-Thermal Analysis**

Figure S4, A1-A3, B1-B3 illustrate normalized  $d(\Delta l)/dT$  values for undamaged, damaged, and self-repair areas plotted as a function of temperature, for OXO-CHI-PUR networks containing OXO-CHI of 1:4, and 1:10 molar ratios, respectively. As seen in Figure S4-A1, the rate of  $d(\Delta l)/dT$  changes with T, and the maximum value is detected at 48 °C, which corresponds to the  $T_g$  values. However, in the damaged area the  $d(\Delta l)/dT$  maximum is lowered to 46 °C, and the width of the  $d(\Delta l)/dT$  values also increase, indicating the lower  $T_g$  values inside the scratch. Upon exposure to UV, the  $d(\Delta l)/dT$  maximum shifts to 50 °C. Similarly, for OXO-CHI-PUR networks containing 1:10 molar ratios OXO-CHI, the  $d(\Delta l)/dT$  maximum at 47 °C decreases to 45 °C upon mechanical damage, but remain unchanged when exposed to UV.

### Model OXO-CHI Macromonomer Experiments

Figure S5 illustrate IRIRI images of OXO-CHI-PUR networks (HDI:PEG:OXO-CHI:DBTDL =1.0:1.33:1.17x10<sup>-4</sup>:2x10<sup>-5</sup>) containing 1:4 molar OXO-CHI recorded as a UV exposure time 0, 60, and 90 min, respectively. (A1-A3) images were obtained by tuning into the 1545 cm<sup>-1</sup> band; (A1'-A3', A1''-A3'', A1'''-A3''') IR spectra recorded from mechanically damaged and undamaged areas.

Figure S6 illustrates IRIRI images of OXO-CHI-PUR networks (HDI:PEG:OXO-CHI:DBTDL =1.0:1.33:1.17x10<sup>-4</sup>:2x10<sup>-5</sup>) containing 1:10 molar OXO-CHI recorded as a UV exposure time 0, 90, and 120 min, respectively. (A1-A3) images were obtained by tuning into the 1545 cm<sup>-1</sup> band; (A1'-A3', A1''-A3'', A1'''-A3''') IR spectra recorded from mechanically damaged and undamaged areas.

Figure S7 illustrates IRIRI images of OXO-CHI-PUR networks (HDI:PEG:OXO-CHI:DBTDL =1.0:1.33:1.17x10<sup>-4</sup>:2x10<sup>-5</sup>) containing 1:1 molar OXO-CHI at pH=6 recorded as a UV exposure time 0, 30, and 60 min, respectively. (A1-A3) images were obtained by tuning into the 1520 cm<sup>-1</sup> band; (A1'-A3', A1''-A3'') IR spectra recorded from mechanically damaged and undamaged areas.

Figure S8 illustrates IRIRI images of OXO-CHI-PUR networks (HDI:PEG:OXO-CHI:DBTDL =1.0:1.33:1.17x10<sup>-4</sup>:2x10<sup>-5</sup>) containing 1:4 molar OXO-CHI and 1 % w/w HALS recorded as a UV exposure time 0, 240, and 360 min, respectively. (A1-A3) images were obtained by tuning into the 1542 cm<sup>-1</sup> band; (A1'-A3', A1''-A3'', A1'''-A3''') IR spectra recorded from mechanically damaged and undamaged areas.

To determine UV sensitivity of OXO-CHI macromonomer, a series of model experiments were conducted in which OXO-CHI molar ratio was varied from 1:1, 1:4, and 1:10. Figure S9-S11, Traces A, B, and C show ATR FT-IR spectra collected as a function of UV exposure for 0, 60 min and 7 days, respectively, for 1:1, 1:4, and 1:10 OXO-CHI molar ratios. Comparison of Traces A and B in Figure S5 shows that the bands corresponding to amide I as well as -CH<sub>2</sub>-

deformation and  $-C-O-C-$  stretching vibrations of OXO ring at 1585, 1326, and 1080  $\text{cm}^{-1}$ , respectively, decrease upon UV exposure. OXO-CHI with 1:4, and 1:10 molar ratios show the same results, but decrease in band intensity is lower compared to OXO-CHI containing 1:1 OXO-CHI molar ratios. These changes are also pointed out in Figures S9-S11 by arrow directions which depict response of relevant bands. Table S1 lists all IR bands sensitive to UV exposure.

Figures S12-S14, Traces A, B, and C illustrate Raman spectra of OXO-CHI macromonomer for 1:1, 1:4, and 1:10 stoichiometries exposed to the same conditions. Comparison of Traces A and B in Figure S8 shows the increase of the 1336  $\text{cm}^{-1}$  band and decrease of 1117  $\text{cm}^{-1}$  due to oxidation of  $-NH_2$  to  $-NO_2$  and loss of hydrazine, respectively, upon UV exposure. On the other hand, the intensity of 1080, and 900  $\text{cm}^{-1}$  bands due to asymmetric and symmetric  $-C-O-C-$  stretching vibrations of OXO also decrease. Again, the bands at 1042, and 972  $\text{cm}^{-1}$  corresponding to  $-C-O-C-$  stretching vibrations of linear aliphatic ether and  $1^\circ -OH$ , respectively increase. These observations suggest OXO ring opening upon UV exposure. Furthermore, the band at 778  $\text{cm}^{-1}$  increases which signifies conformational chair-to-boat conversion of glycosine units along the CHI-backbone. As shown in Trace C, further UV exposure of OXO-CHI macromonomer resulting amplification of these changes which indicate the continuation of free radical reactions. Figure S9-S10, illustrating Raman spectra of OXO-CHI macromonomer containing 1:4, and 1:10 molar ratios, respectively, showed the same result, although smaller magnitude of band intensities were observed. These changes are also pointed out in Figures S12-S14 by arrow directions which depict response of relevant bands. Table S2 lists all spectroscopic changes of Raman bands resulting from UV exposure.

These ATR FT-IR and Raman analysis of the intensity changes of the vibrational bands sensitive to UV exposure allowed us to identify reactions resulting from UV exposure which are summarized in Figure S15: (a) OXO ring opening, reflected by the decrease of the  $\text{-C-O-C-}$  vibrations at 1080, and 900  $\text{cm}^{-1}$ ,  $\text{-CH}_2\text{-}$  deformation mode of OXO-ring at 1326  $\text{cm}^{-1}$ ; (b) chain scission of the  $\text{-C-O-C-}$  segments shown by the increase of the linear  $\text{-C-O-C-}$  stretching vibrations at 1042; (c) the chair-to-boat conformational changes of pyranose units of CHI reflected by the increase of the 778  $\text{cm}^{-1}$  band; (d)  $\text{NH}_2$  oxidation, leading to the formation of  $\text{NO}_2$  shown by the decrease of amide I band at 1580  $\text{cm}^{-1}$  band as well as increase of 1336  $\text{cm}^{-1}$  band corresponding to  $\text{-NO}_2$  and (e) the formation of hydrazine manifested by the appearance of the band at 1117  $\text{cm}^{-1}$ .

## Figures and Legends

Figure S1. Synthetic steps involved in the formation of OXO-CHI-PUR networks; 1) Reactions of OXO with CHI leading to the formation of OXO-CHI macromonomer; 2) Reactions of OXO-CHI with HDI and PEG leading to formations of OXO-CHI-PUR network.

Figure S2. ATR FT-IR spectra of CHI and OXO-CHI macromonomer.

Figure S3.  $^{13}\text{C}$  NMR spectra of A) CHI, and B) OXO-CHI macromonomer.

Figure S4. Plot of  $d(\Delta I)/dT$  vs temperature of OXO-CHI-PUR network (HDI:PEG:OXO-CHI:DBTDL = 1.0:1.33:1.17x10<sup>-4</sup>:2x10<sup>-5</sup>) containing OXO-CHI of 1:4 (A1-A3), and 1:10 (B1-B3) molar ratios, respectively.

Figure S5. IRIRI images of OXO-CHI-PUR networks (HDI:PEG:OXO-CHI:DBTDL = 1.0:1.33:1.17x10<sup>-4</sup>:2x10<sup>-5</sup>) containing 1:4 molar OXO-CHI recorded as a UV exposure time 0, 60, and 90 min, respectively. (A1-A3) images were obtained by tuning into the 1545 cm<sup>-1</sup> band; (A1'-A3', A1''-A3'', A1'''-A3''') IR spectra recorded from mechanically damaged and undamaged areas.

Figure S6. IRIRI images of OXO-CHI-PUR networks (HDI:PEG:OXO-CHI:DBTDL = 1.0:1.33:1.17x10<sup>-4</sup>:2x10<sup>-5</sup>) containing 1:10 molar OXO-CHI recorded as a UV exposure time 0, 90, and 120 min, respectively. (A1-A3) images were obtained by tuning into the 1545 cm<sup>-1</sup> band; (A1'-A3', A1''-A3'', A1'''-A3''') IR spectra recorded from mechanically damaged and undamaged areas.

Figure S7. IRIRI images of OXO-CHI-PUR networks (HDI:PEG:OXO-CHI:DBTDL = 1.0:1.33:1.17x10<sup>-4</sup>:2x10<sup>-5</sup>) containing 1:1 molar OXO-CHI at pH=6 recorded as a UV exposure time 0, 30, and 60 min, respectively. (A1-A3) images were obtained by tuning into the 1520 cm<sup>-1</sup> band; (A1'-A3', A1''-A3'') IR spectra recorded from mechanically damaged and undamaged areas.

Figure S8. IRIRI images of OXO-CHI-PUR networks (HDI:PEG:OXO-CHI:DBTDL =1.0:1.33:1.17x10<sup>-4</sup>:2x10<sup>-5</sup>) containing 1:4 molar OXO-CHI and 1 % w/w HALS recorded as a UV exposure time 0, 240, and 360 min, respectively. (A1-A3) images were obtained by tuning into the 1542 cm<sup>-1</sup> band; (A1'-A3', A1''-A3'', A1'''-A3''') IR spectra recorded from mechanically damaged and undamaged areas.

Figure S9. ATR FT-IR spectra of OXO-CHI (1:1), before (A), after 60 min of UV exposure (B), and 7 days later (C) of UV exposure; arrow directions point out increasing (↑) and decreasing (↓) intensities of relevant bands.

Figure S10. ATR FT-IR spectra of OXO-CHI (1:4), before (A), after 60 min of UV exposure (B), and 7 days later (C) of UV exposure; arrow directions point out increasing (↑) and decreasing (↓) intensities of relevant bands.

Figure S11. ATR FT-IR spectra of OXO-CHI (1:10), before (A), after 60 min of UV exposure (B), and 7 days later (C) of UV exposure; arrow directions point out increasing (↑) and decreasing (↓) intensities of relevant bands.

Figure S12. Raman spectra of OXO-CHI (1:1), before (A), after 60 min of UV exposure (B), and 7 days later (C) of UV exposure; arrow directions point out increasing (↑) and decreasing (↓) intensities of relevant bands.

Figure S13. Raman spectra of OXO-CHI (1:4), before (A), after 60 min of UV exposure (B), and 7 days later (C) of UV exposure; arrow directions point out increasing (↑) and decreasing (↓) intensities of relevant bands.

Figure S14. Raman spectra of OXO-CHI (1:10), before (A), after 60 min of UV exposure (B), and 7 days later (C) of UV exposure; arrow directions point out increasing (↑) and decreasing (↓) intensities of relevant bands.

Figure S15. Schematic diagram of reaction products and band assignments obtained from UV exposure of OXO-CHI.

Table S1. Vibrational bands observed in IR measurements 1:1, 1:4, and 1:10 OXO-CHI molar ratios. Arrows  $\uparrow\downarrow$  indicate band increase or decrease for a given OXO-CHI ratio.

Table S2. Vibrational bands observed in Raman measurements for 1:1, 1:4, and 1:10 OXO-CHI molar ratios. Arrows  $\uparrow\downarrow$  indicate band increase or decrease for a given OXO-CHI ratio.

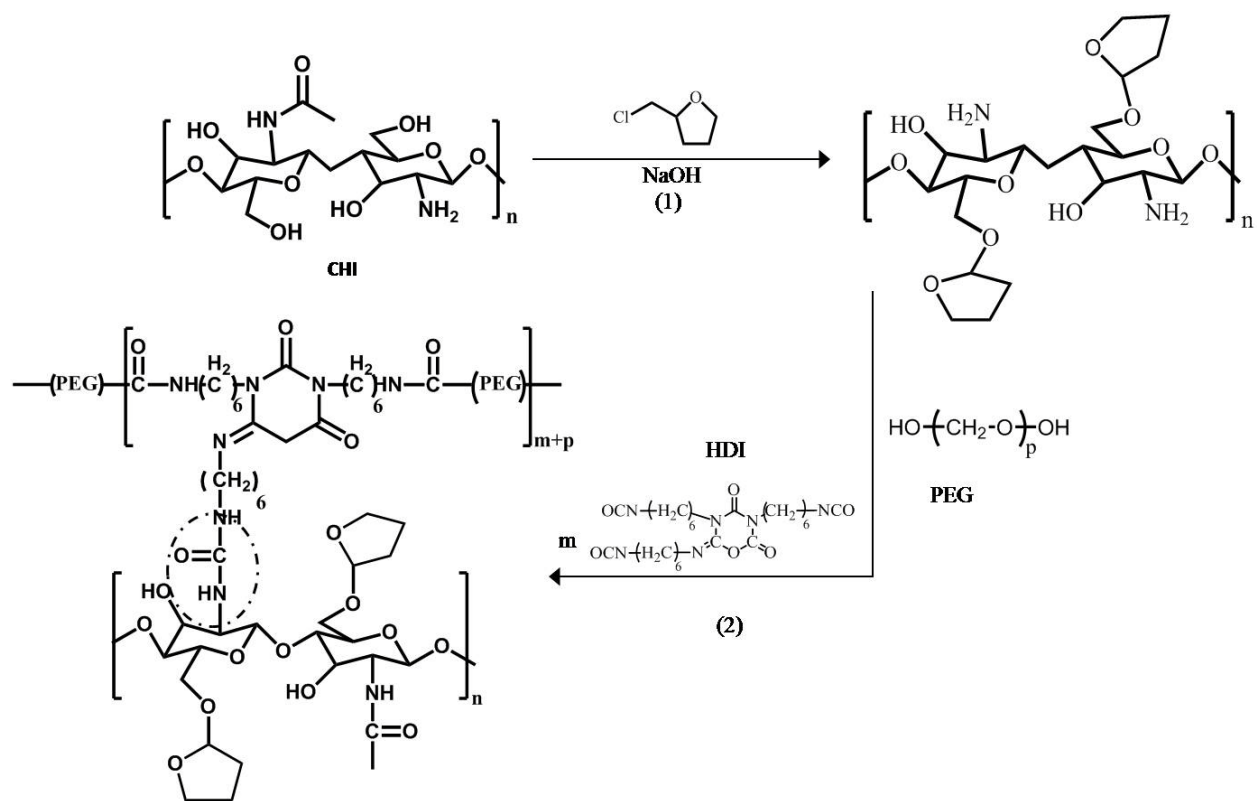


Figure S1.

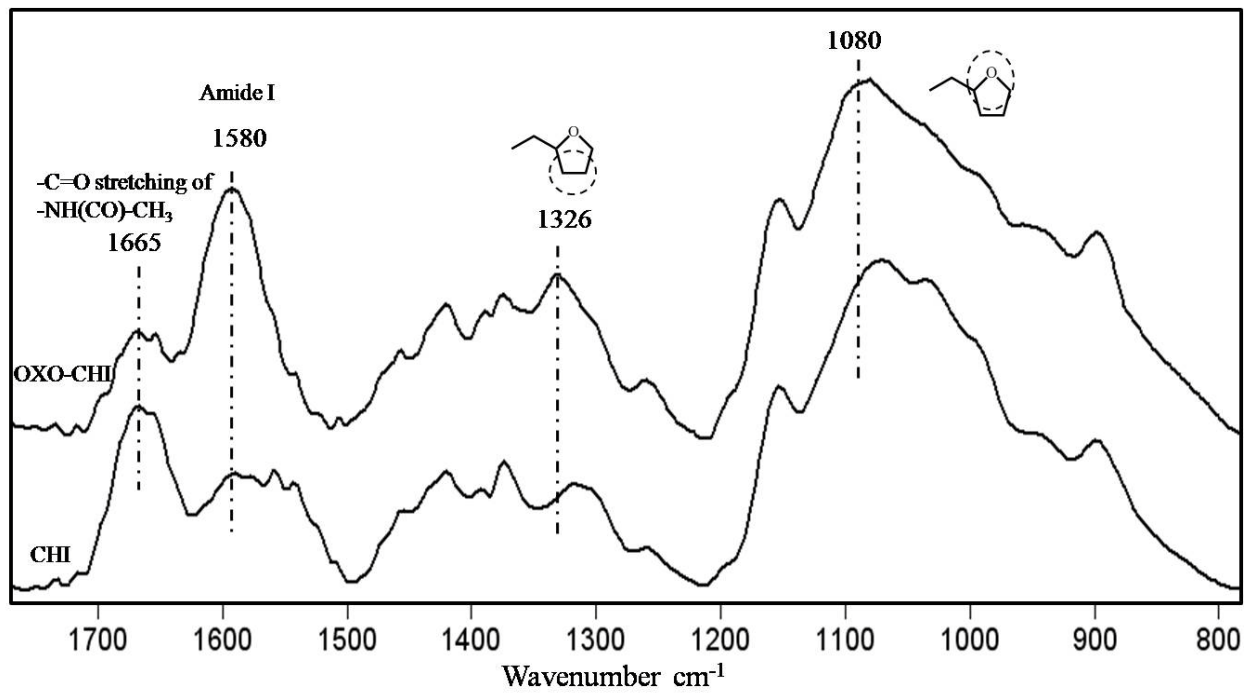


Figure S2.

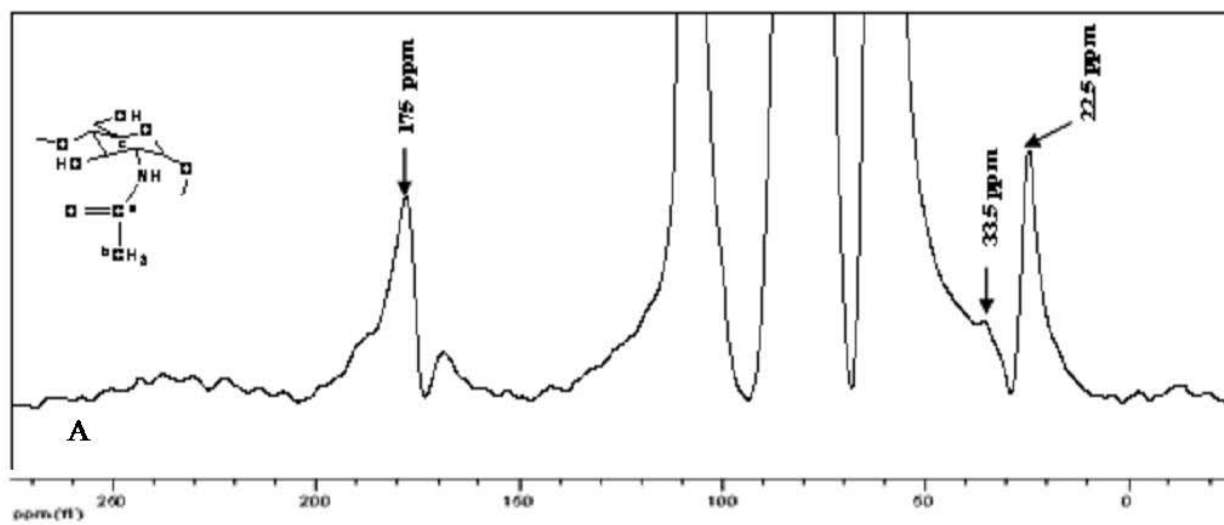
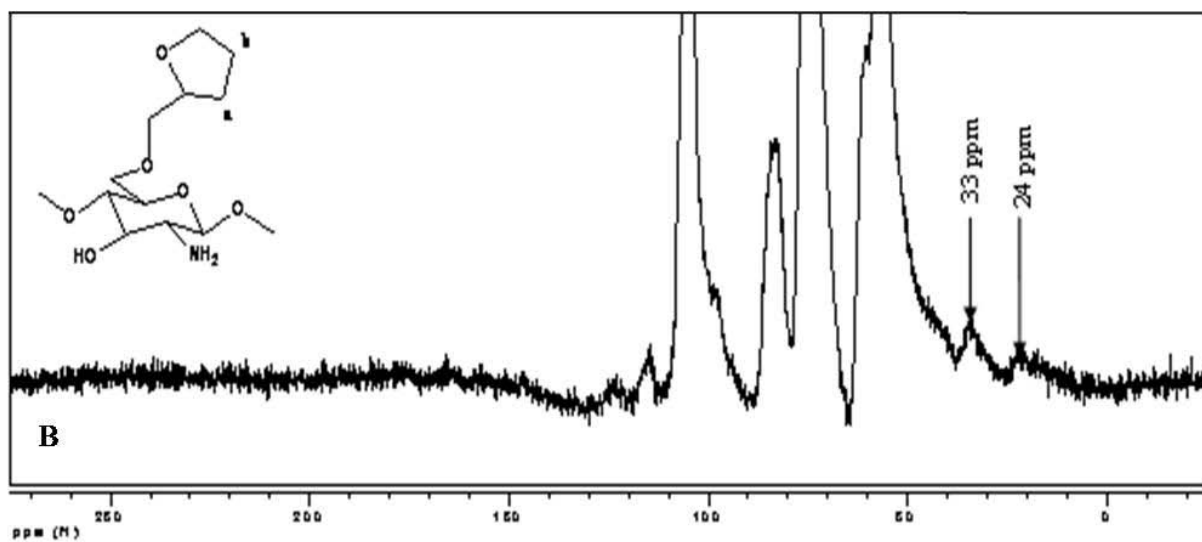


Figure S3.

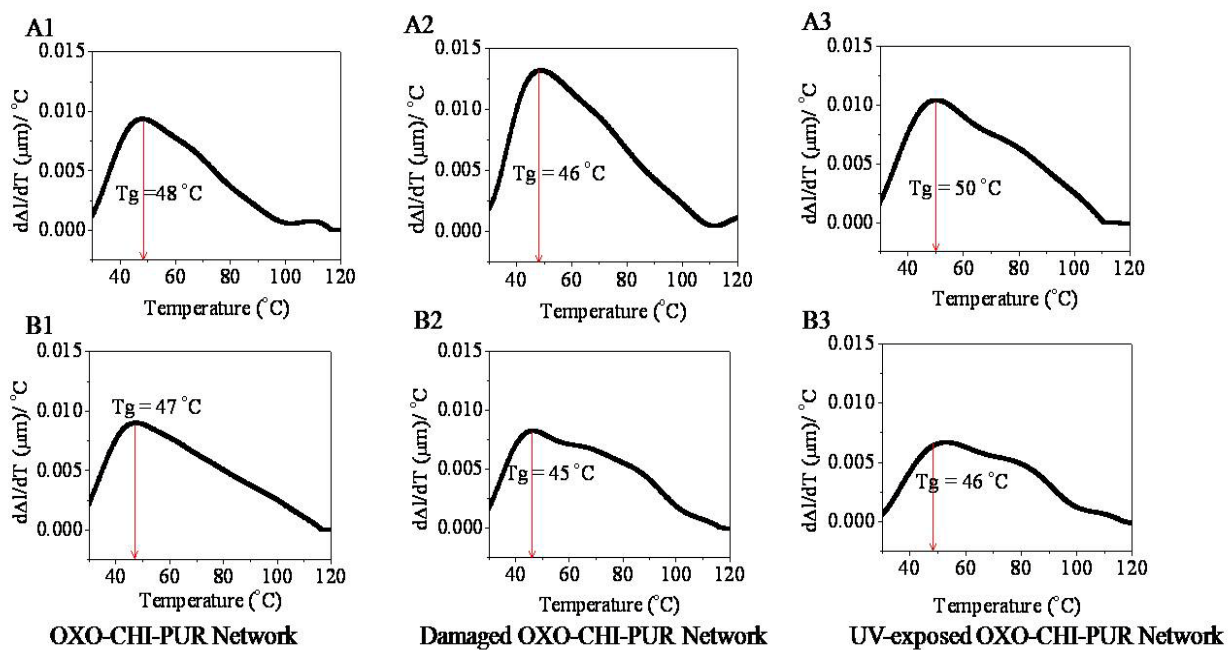


Figure S4.

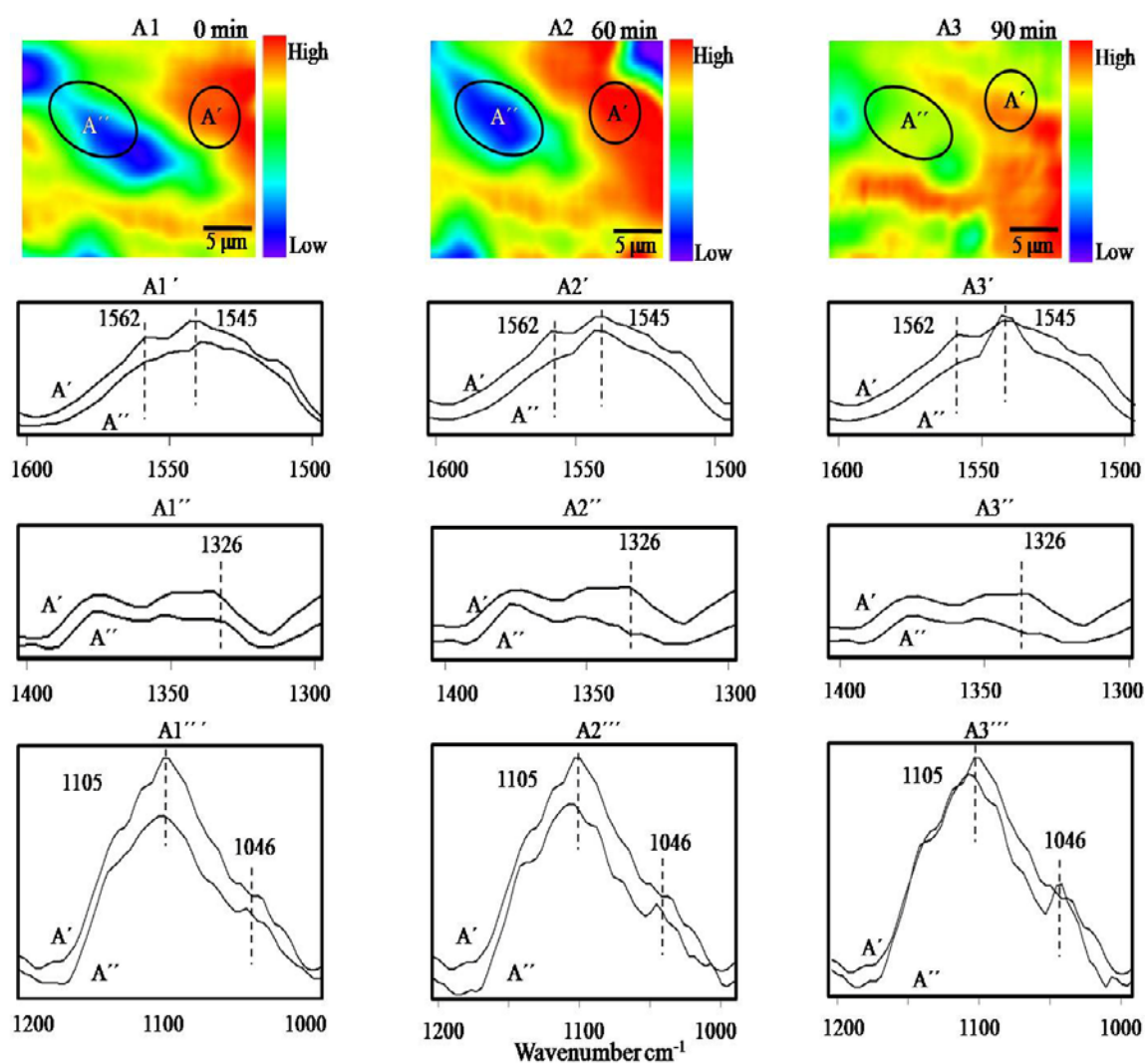


Figure S5.

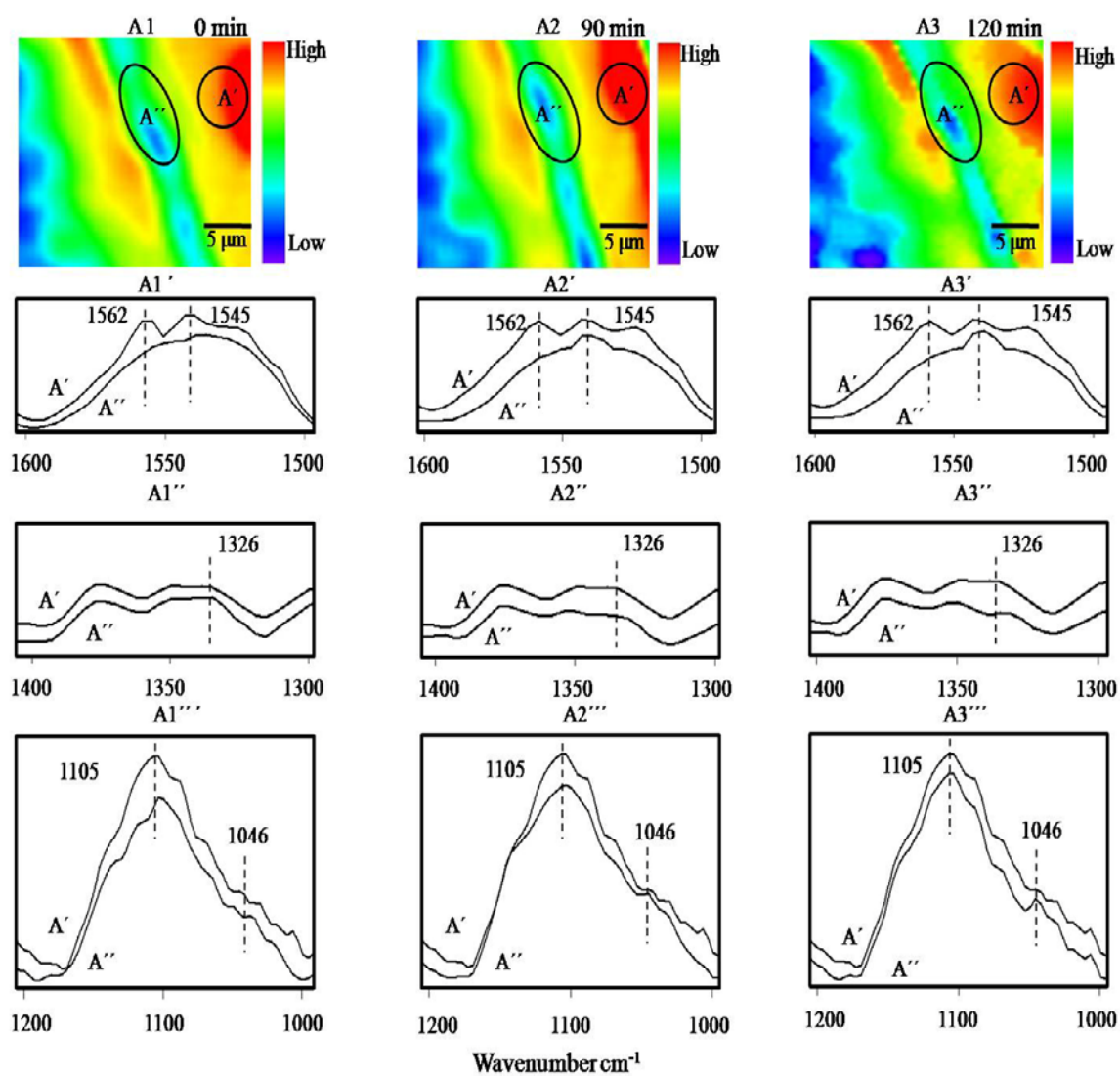


Figure S6.

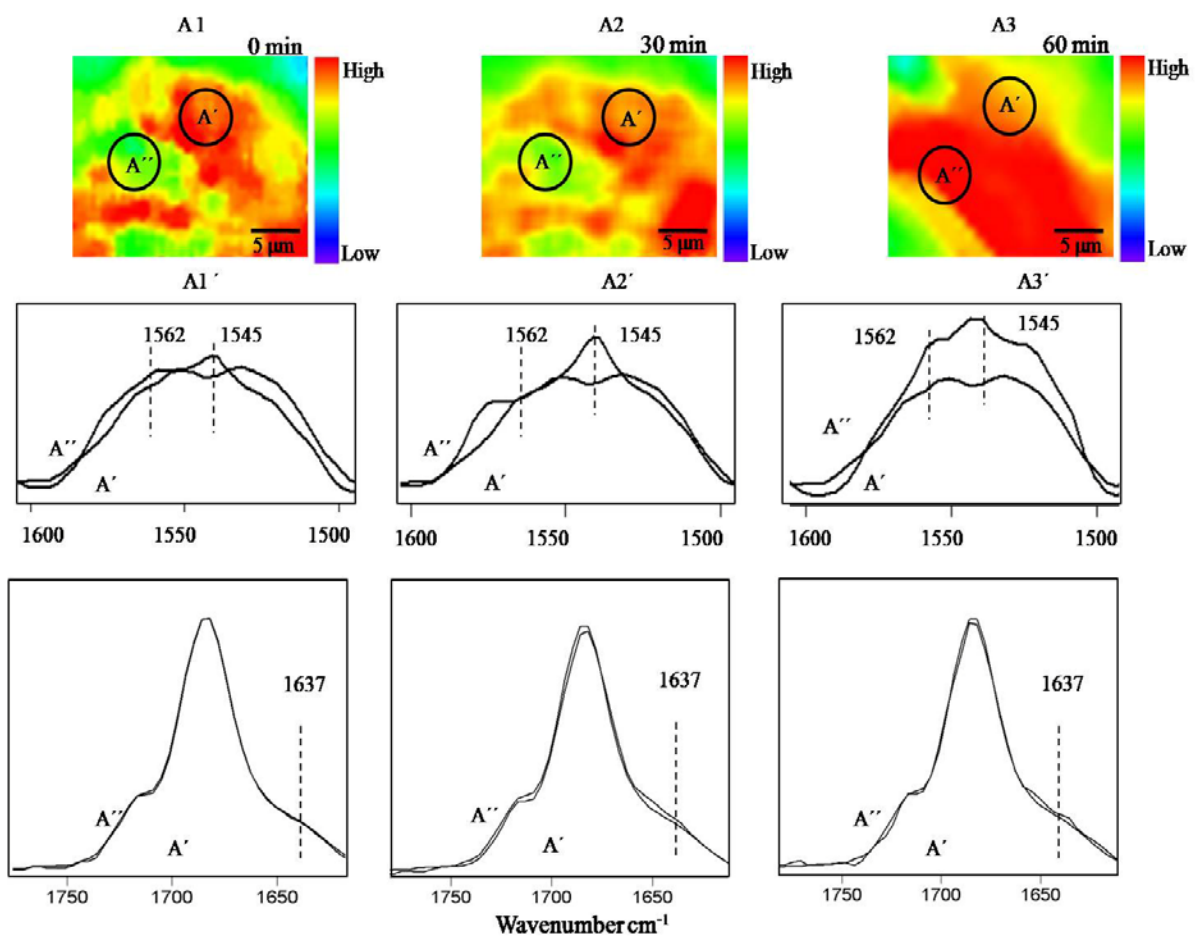


Figure S7.

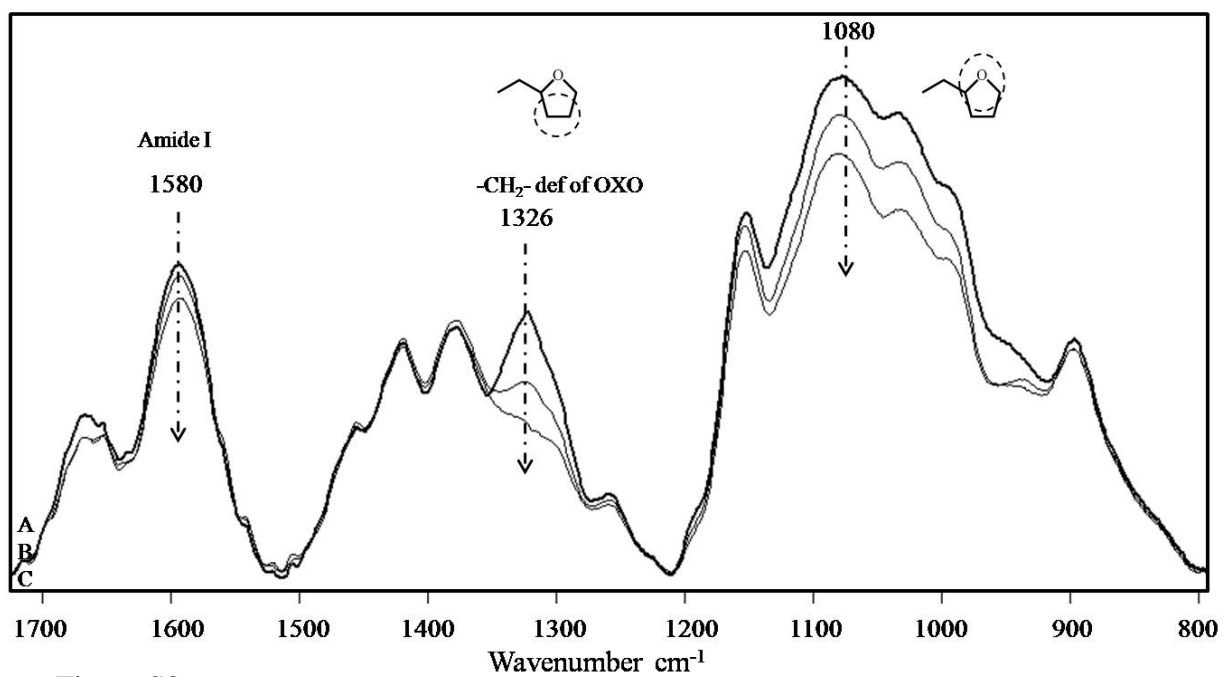


Figure S8.

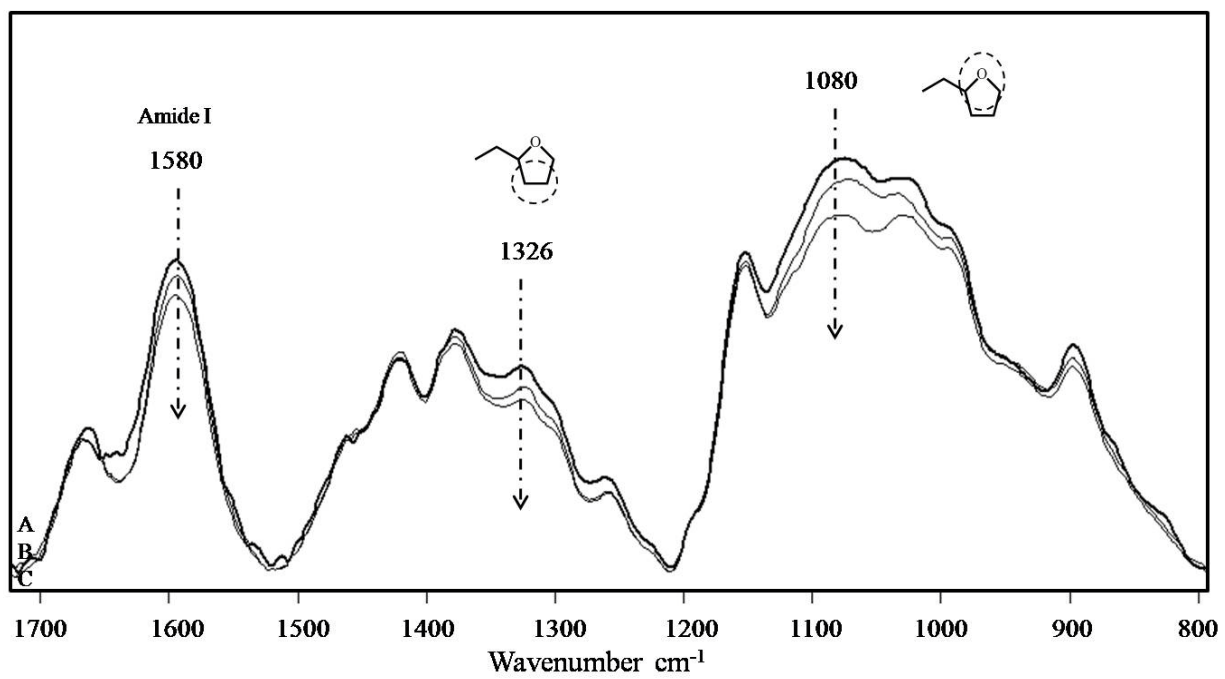


Figure S9.

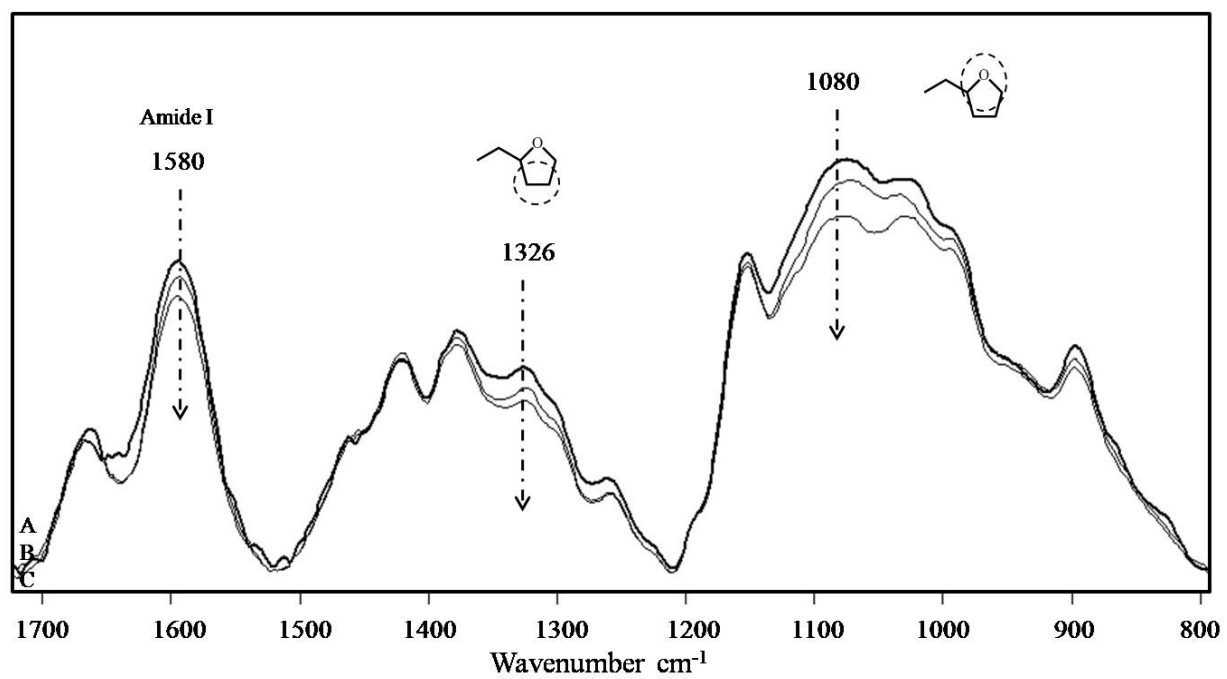


Figure S10.

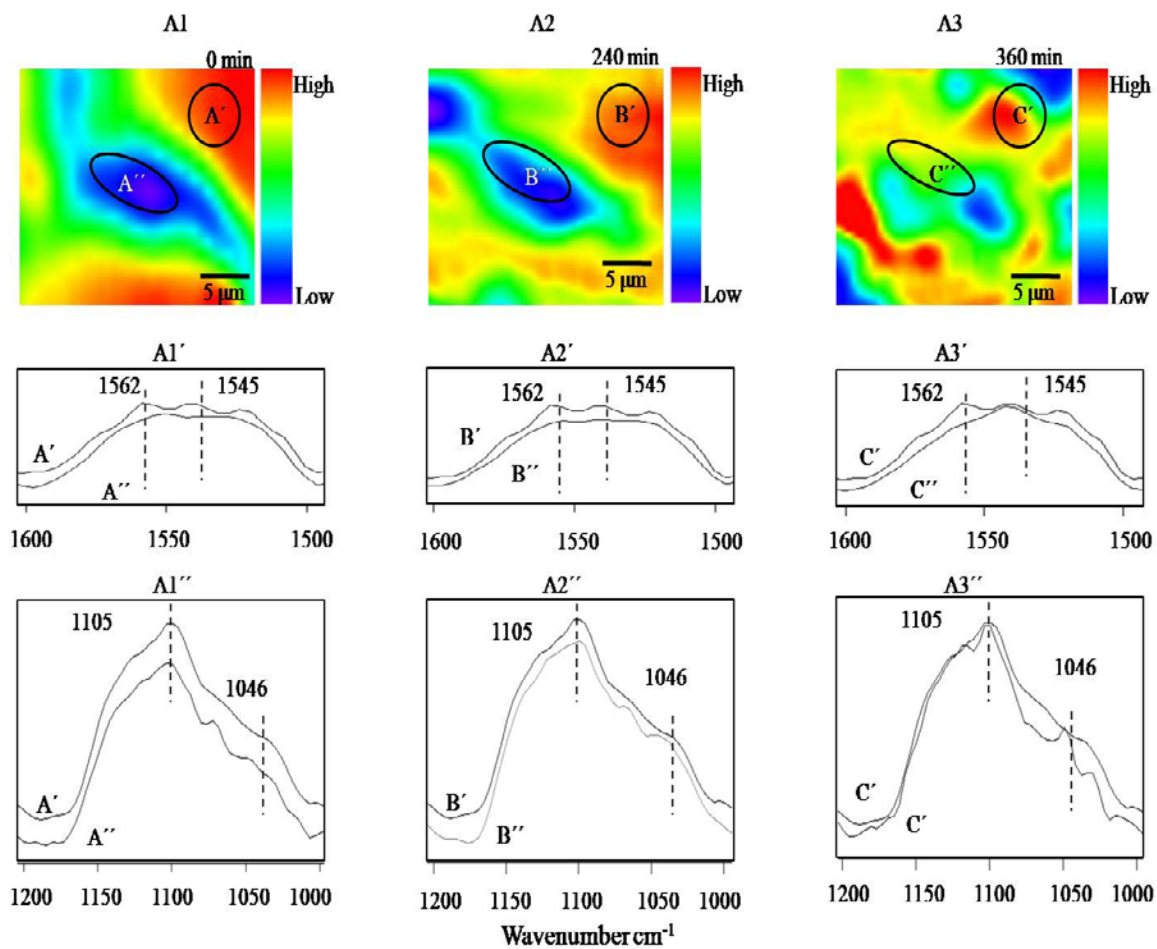


Figure S11.

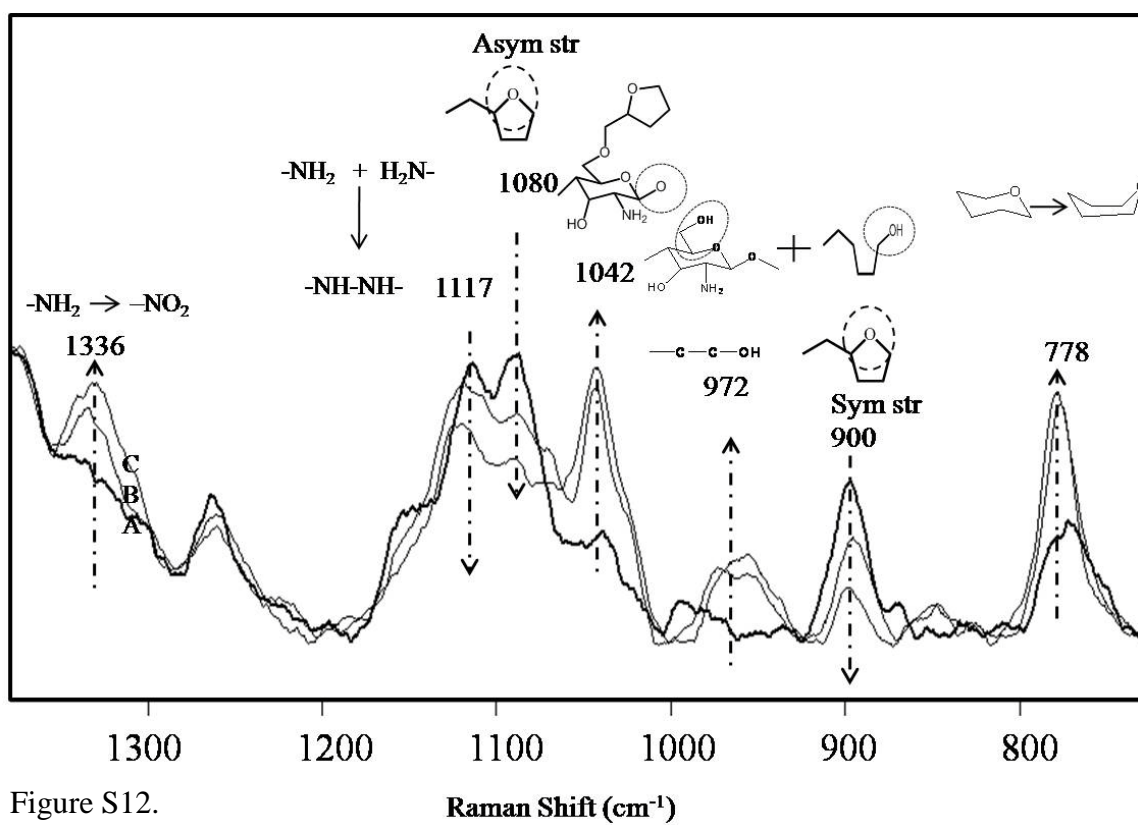


Figure S12.

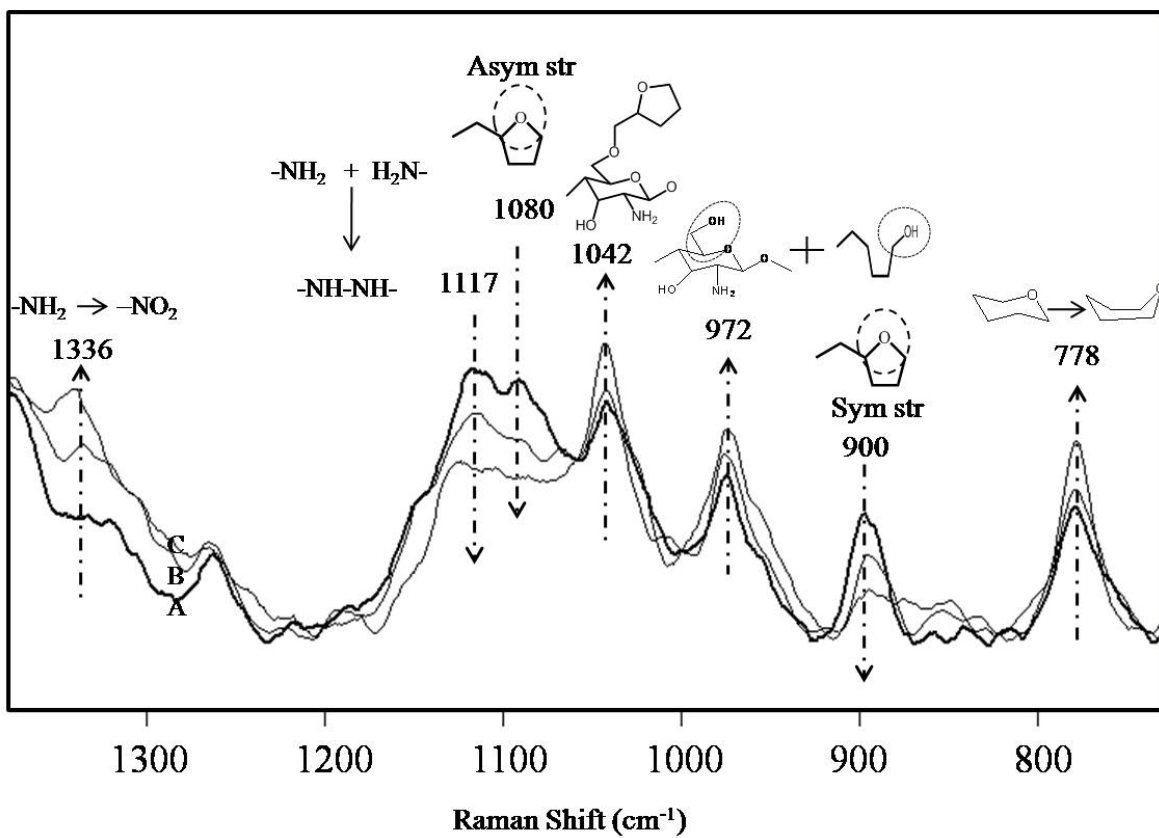


Figure S13.

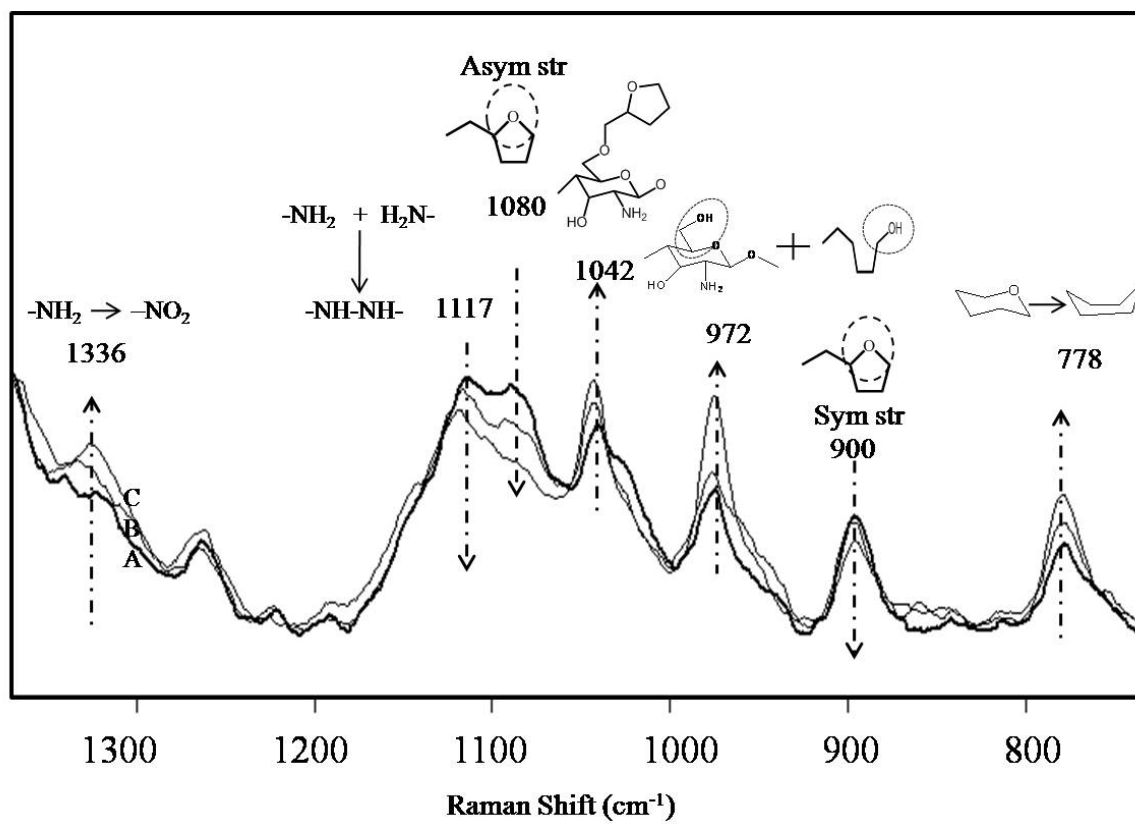


Figure S14.

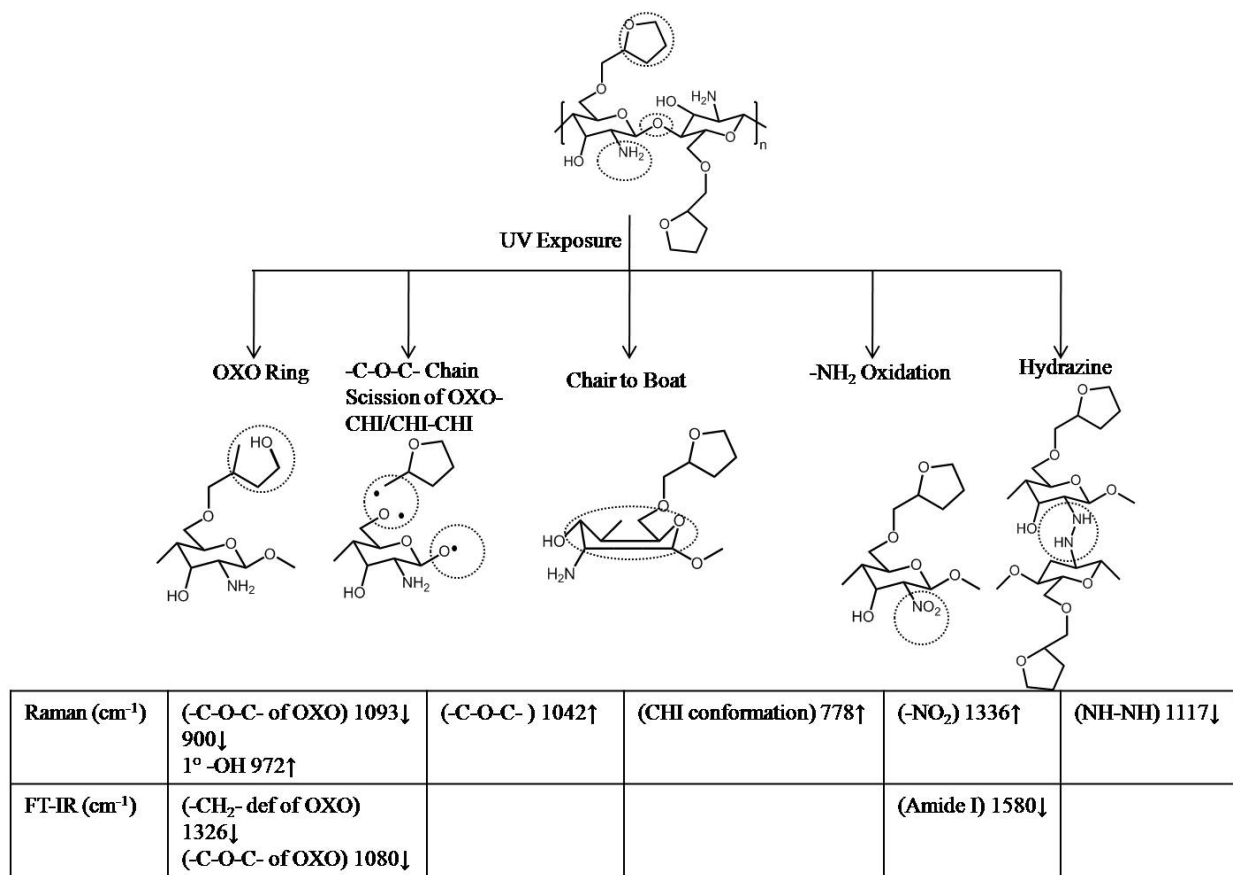


Figure S15.

<i>IR</i> <i>OXO-CHI</i>	1580 cm <sup>-1</sup> Amide I	1326 cm <sup>-1</sup> -CH <sub>2</sub> - def of OXO	1080 cm <sup>-1</sup> -C-O-C- stretch of OXO
1:1	↓	↓	↓
1:4	↓	↓	↓
1:10	↓	↓	↓

Table S1.

Raman OXO-CHI	1336 cm <sup>-1</sup> -NO <sub>2</sub>	1117 cm <sup>-1</sup> 	1080 cm <sup>-1</sup> Asym -C-O-C- stretch of OXO	1042 cm <sup>-1</sup> -C-O-C- of CHI-CHI	972 cm <sup>-1</sup> 1° -OH	900 cm <sup>-1</sup> Sym -C-O-C- stretch of OXO	778 cm <sup>-1</sup> Chair-to-boat
1:1	↑	↓	↓	↑	↑	↓	↑
1:4	↑	↓	↓	↑	↑	↓	↑
1:10	↑	↓	↓	↑	↑	↓	↑

Table S2.